

## Finite Rotation Piezoelectric Exact Geometry Solid-Shell Element with Nine Degrees of Freedom per Node

G. M. Kulikov<sup>1</sup> and S. V. Plotnikova<sup>1</sup>

**Abstract:** This paper presents a robust non-linear piezoelectric exact geometry (EG) four-node solid-shell element based on the higher-order 9-parameter equivalent single-layer (ESL) theory, which permits one to utilize 3D constitutive equations. The term EG reflects the fact that coefficients of the first and second fundamental forms of the reference surface are taken exactly at each element node. The finite element formulation developed is based on a new concept of interpolation surfaces (I-surfaces) inside the shell body. We introduce three I-surfaces and choose nine displacements of these surfaces as fundamental shell unknowns. Such choice allows us to represent the finite rotation piezoelectric higher-order EG solid-shell element formulation in a very compact form and to utilize in curvilinear reference surface coordinates the strain-displacement relationships, which are objective, that is, invariant under arbitrarily large rigid-body shell motions. To avoid shear and membrane locking and have no spurious zero energy modes, the assumed displacement-independent strain and stress resultant fields are introduced. In this connection, the Hu-Washizu variational equation is invoked. To implement the analytical integration throughout the element, the modified ANS method is applied. As a result, the present finite rotation piezoelectric EG solid-shell element formulation permits the use of coarse meshes and very large load increments.

**Keywords:** Piezoelectric laminated shell, exact geometry solid-shell element, non-linear 9-parameter shell model

### 1 Introduction

In recent years, a considerable progress has been achieved on the development of continuum-based finite elements [Tan and Vu-Quoc (2005), Klinkel and Wagner (2006, 2008), Lentzen (2009)] that can handle the geometrically non-linear analysis of thin piezoelectric laminated composite shells satisfactorily. These elements

---

<sup>1</sup> Department of Applied Mathematics and Mechanics, Tambov State Technical University, Tambov 392000, Russia, kulikov@apmath.tstu.ru

are typically defined by two layers of nodes at the bottom and top surfaces of the shell with three displacement degrees of freedom per node and known as isoparametric 6-parameter piezoelectric solid-shell elements. Unfortunately, a 6-parameter solid-shell element formulation based on the complete 3D constitutive equations is deficient because thickness locking occurs. This is due to the fact that the linear displacement field in the thickness direction results in a constant transverse normal strain, which in turn causes artificial stiffening of the shell element in the case of non-vanishing Poisson's ratios. It should be mentioned that the errors caused by thickness locking do not decrease with the mesh refinement because the reason of stiffening lies in the shell theory itself rather than the finite element discretization. To prevent thickness locking, the transverse normal strain is enriched in the thickness direction by a linear term as suggested by Buchter, Ramm and Roehl (1994).

Another popular way of using 3D constitutive equations is to employ higher-order shell models, as a rule, with seven displacement degrees of freedom for the non-linear analysis of purely mechanical shell problems [Parisch (1995), Sansour (1995), El-Abbasi and Meguid (2000), Brank (2005), Arciniega and Reddy (2007), Kulikov and Carrera (2008), Kulikov and Plotnikova (2008a), Brank, Ibragimbegovic and Bohinc (2008), Lee and Lee (2008)]. It is well-known that a conventional way for developing the higher-order shell formulation is to utilize either quadratic or cubic series expansions in the thickness coordinate and to choose as unknowns the generalized displacements of the midsurface. Herein, the 9-parameter piezoelectric laminated shell model is developed for the first time using a new concept of interpolation surfaces (I-surfaces) inside the shell body [Kulikov and Carrera (2008), Kulikov and Plotnikova (2008a)]. We introduce three equally located I-surfaces, namely, bottom, middle and top and choose the values of displacements with correspondence to these surfaces as fundamental shell unknowns. Such choice of displacements with the consequent use of the Lagrange polynomials of the second order in the thickness direction permits one to represent the finite rotation higher-order 9-parameter shell formulation developed in a very compact form and to utilize non-linear strain-displacement equations, which are completely free for arbitrarily large rigid-body shell motions. Taking into account that displacement vectors of I-surfaces are resolved in the reference surface frame the proposed higher-order shell formulation is very promising for developing the high performance piezoelectric EG solid-shell elements. The term EG reflects the fact that the parametrization of the reference surface is known and, therefore, coefficients of the first and second fundamental forms are taken exactly at element nodes, which are employed in innovative analytical integration schemes proposed by Kulikov and Plotnikova (2006, 2007, 2009).

It is assumed that the electric potential is linear through the thickness of the piezo-

electric layer and all displacement and electric potential degrees of freedom are coupled via 3D constitutive equations. The first assumption means that the electric field is constant through the thickness of the piezoelectric layer, which is in bending dominated situations not correct [see, e.g. Sze, Yang and Fan (2004)]. Besides, in such case the electric charge conservation law never can be satisfied precisely. The analytical developments for piezoelectric beams [Gopinathan, Varadan and Varadan (2000)] and plates [Benjeddou, Deü and Letombe (2002)] showed that the quadratic variation of the electric potential in the thickness direction is sufficient to solve this problem. However, the quadratic approximation of the electric potential leads to including additional degrees of freedom in a finite element formulation and seems to be excessive for the actuator shell analysis that is discussed in the present paper.

To avoid shear and membrane locking and have no spurious zero energy modes, the assumed displacement-independent strain and stress resultant fields are invoked. This approach was developed for the finite rotation 6-parameter EG shell element formulations by Kulikov and Plotnikova (2002, 2004, 2006). Herein, the above hybrid stress-strain formulation is generalized to the finite rotation piezoelectric EG four-node solid-shell element based on the higher-order 9-parameter shell model. The proposed piezoelectric EG solid-shell element formulation has computational advantages compared to conventional piezoelectric isoparametric solid-shell element formulations since it reduces the computational cost of numerical integration in the evaluation of the tangent stiffness matrix. This is due to the facts that, first, all element matrices require only direct substitutions, i.e., no expensive numerical matrix inversion is needed. The latter is unusual for the hybrid/mixed isoparametric shell element formulations [e.g. Klinkel and Wagner (2006)]. Second, we use the efficient 3D analytical integration that permits to employ coarse meshes. Finally, the hybrid stress-strain piezoelectric EG solid-shell element developed allows one to utilize load increments, which are much larger than possible with existing piezoelectric isoparametric solid-shell elements [e.g. Tan and Vu-Quoc (2005)]. Therefore, large-scale computations for thick piezoelectric laminated shell structures undergoing finite rotations can be carried out efficiently with the help of the proposed higher-order hybrid stress-strain EG four-node solid-shell element.

## 2 Kinematic description of shell

Consider a shell built up in the general case by the arbitrary superposition across the wall thickness of  $N$  layers of the uniform thickness  $h_n = z_n - z_{n-1}$  including the  $\ell$ th piezoelectric layer (PZT) as shown in Figure 1. The  $n$ th layer may be defined as a 3D body of volume  $V_n$  bounded by two surfaces  $\Omega_{n-1}$  and  $\Omega_n$ , located at the distances  $|z_{n-1}|$  and  $|z_n|$  measured with respect to the reference surface  $\Omega$ , and the

edge boundary surface  $\Sigma_n$ . It is supposed that the reference surface  $\Omega$  is continuous, sufficiently smooth and without any singularities [see discussion on this subject in Kulikov and Plotnikova (2007)]. Let the reference surface be referred to the orthogonal curvilinear coordinates  $\theta_1$  and  $\theta_2$ , which are referred to the lines of principal curvatures of its surface, whereas the coordinate  $\theta_3$  is oriented along the unit vector  $\mathbf{e}_3$  normal to the reference surface;  $\mathbf{e}_1$  and  $\mathbf{e}_2$  are the unit vectors tangent to the lines of principal curvatures. As I-surfaces, we choose bottom  $\Omega^-$ , middle  $\Omega^M$  and top  $\Omega^+$  surfaces of the shell. Here and in the following developments, the index  $n$  identifies the belonging of any quantity to the  $n$ th layer and runs from 1 to  $N$ ; the index of the piezoelectric layer  $\ell = i_1, i_2, \dots, i_L$ , where  $L$  is the number of piezoelectric layers bonded to the outer surfaces of the host structure or embedded into its body; Greek indices  $\alpha, \beta$  range from 1 to 2; indices  $i, j, m$  range from 1 to 3; the superscripts  $I, J$  identify the belonging of any quantity to the I-surfaces and take values  $-$ ,  $M$  and  $+$ .

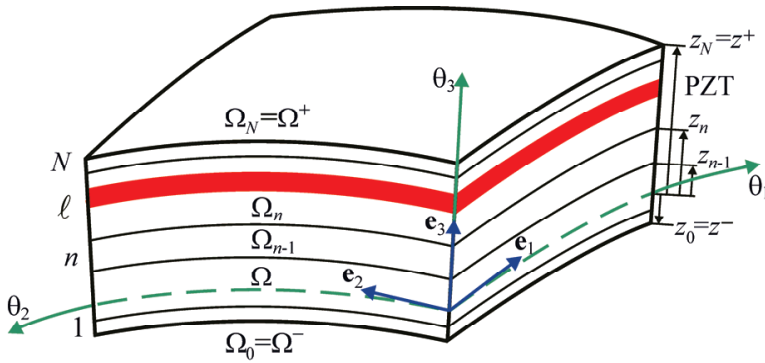


Figure 1: Laminated shell with embedded piezoelectric layer (PZT)

The displacement field is approximated in the thickness direction according to [Kulikov (2001)]:

$$\mathbf{u} = \sum_I L^I \mathbf{u}^I, \tag{1}$$

where  $\mathbf{u}^I(\theta_1, \theta_2)$  are the displacement vectors of I-surfaces;  $L^I(\theta_3)$  are the Lagrange polynomials of the second order defined as

$$L^- = \frac{2}{h^2} (z^M - \theta_3) (z^+ - \theta_3),$$

$$L^M = \frac{4}{h^2} (\theta_3 - z^-) (z^+ - \theta_3),$$

$$L^+ = \frac{2}{h^2} (\theta_3 - z^-) (\theta_3 - z^M), \quad (2)$$

where  $h = z^+ - z^-$  is the thickness of the shell;  $z^- = z_0$ ,  $z^M = (z_0 + z_N)/2$  and  $z^+ = z_N$  are the transverse coordinates of I-surfaces of the shell.

Next, we represent the displacement vectors of I-surfaces as follows:

$$\mathbf{u}^I = \sum_i u_i^I \mathbf{e}_i, \quad (3)$$

where  $u_i^I(\theta_1, \theta_2)$  are the components of displacement vectors of I-surfaces in the orthonormal reference surface basis  $\mathbf{e}_i$ .

Therefore, the strain-displacement relationships of the 9-parameter shell model [Kulikov and Plotnikova (2008a)] can be written as

$$\varepsilon_{ij} = \sum_I L^I \varepsilon_{ij}^I. \quad (4)$$

Here,  $\varepsilon_{ij}^I(\theta_1, \theta_2)$  are the components of the Green-Lagrange strain tensor of I-surfaces given by

$$\begin{aligned} 2\varepsilon_{\alpha\beta}^I &= c_\alpha^I \lambda_{\alpha\beta}^I + c_\beta^I \lambda_{\beta\alpha}^I + \sum_i \lambda_{i\alpha}^I \lambda_{i\beta}^I, \\ 2\varepsilon_{\alpha 3}^I &= c_\alpha^I \beta_\alpha^I + \lambda_{3\alpha}^I + \sum_i \beta_i^I \lambda_{i\alpha}^I, \\ 2\varepsilon_{33}^I &= 2\beta_3^I + \sum_i \beta_i^I \beta_i^I, \end{aligned} \quad (5)$$

where

$$\begin{aligned} \lambda_{\alpha\alpha}^I &= \frac{1}{A_\alpha} u_{\alpha,\alpha}^I + B_\beta u_\beta^I + k_\alpha u_3^I \text{ for } \beta \neq \alpha, \\ \lambda_{\beta\alpha}^I &= \frac{1}{A_\alpha} u_{\beta,\alpha}^I - B_\beta u_\alpha^I \text{ for } \beta \neq \alpha, \\ \lambda_{3\alpha}^I &= \frac{1}{A_\alpha} u_{3,\alpha}^I - k_\alpha u_\alpha^I, \quad \beta_i^- = \frac{1}{h} (-3u_i^- + 4u_i^M - u_i^+), \\ \beta_i^M &= \frac{1}{h} (-u_i^- + u_i^+), \quad \beta_i^+ = \frac{1}{h} (u_i^- - 4u_i^M + 3u_i^+), \\ c_\alpha^I &= 1 + k_\alpha z^I, \quad B_\alpha = \frac{1}{A_\alpha A_\beta} A_{\beta,\alpha} \text{ for } \beta \neq \alpha, \end{aligned} \quad (6)$$

where  $A_\alpha$  and  $k_\alpha$  are the coefficients of the first fundamental form and principal curvatures of the reference surface;  $c_\alpha^I$  are the components of the shifter tensor at I-surfaces of the shell; the abbreviation  $(\cdot)_{,\alpha}$  implies the partial derivatives with respect to coordinates  $\theta_\alpha$ . It is noteworthy that strain-displacement relationships (4) and (5) exactly represent arbitrarily large rigid-body shell motions in a convected curvilinear coordinate system [Kulikov and Plotnikova (2008a)].

### 3 Description of electric field

The electric potential inside the  $\ell$ th piezoelectric layer is assumed to be linear in the thickness direction

$$\varphi_\ell = N_\ell^- \varphi_\ell^- + N_\ell^+ \varphi_\ell^+, \tag{7}$$

$$N_\ell^- = \frac{1}{h_\ell} (z_\ell - \theta_3), \quad N_\ell^+ = \frac{1}{h_\ell} (\theta_3 - z_{\ell-1}), \tag{8}$$

where  $\varphi_\ell^- (\theta_1, \theta_2)$  and  $\varphi_\ell^+ (\theta_1, \theta_2)$  are the values of the electric potential on the bottom and top surfaces of the  $\ell$ th layer;  $h_\ell = z_\ell - z_{\ell-1}$  is the thickness of the piezoelectric layer.

The relation between the electric field  $\mathbf{E}^{(\ell)}$  and the electric potential  $\varphi_\ell$  is given by

$$\mathbf{E}^{(\ell)} = -\nabla \varphi_\ell, \tag{9}$$

that is,

$$E_\alpha^{(\ell)} = N_\ell^- E_\alpha^{(\ell)-} + N_\ell^+ E_\alpha^{(\ell)+}, \quad E_3^{(\ell)} = -\frac{1}{h_\ell} (\varphi_\ell^+ - \varphi_\ell^-),$$

$$E_\alpha^{(\ell)-} = -\frac{1}{A_\alpha} \varphi_{\ell,\alpha}^-, \quad E_\alpha^{(\ell)+} = -\frac{1}{A_\alpha} \varphi_{\ell,\alpha}^+, \tag{10}$$

where  $E_\alpha^{(\ell)-}$  and  $E_\alpha^{(\ell)+}$  are the tangential components of the electric field of outer surfaces of the  $\ell$ th layer. It is seen that the normal component of the electric field  $E_3^{(\ell)}$  is constant through the thickness of the piezoelectric layer. A short discussion on that is presented in Introduction.

### 4 Constitutive equations of piezoelectricity

The constitutive equations of linear piezoelectricity for the monoclinic piezoelectric layer with reflectional symmetry in surfaces parallel to the reference surface can be expressed as

$$\boldsymbol{\varepsilon} = \mathbf{A}^{(\ell)} \boldsymbol{\sigma}^{(\ell)} + \left( \mathbf{d}^{(\ell)} \right)^T \mathbf{E}^{(\ell)}, \tag{11}$$

$$\mathbf{D}^{(\ell)} = \mathbf{d}^{(\ell)} \boldsymbol{\sigma}^{(\ell)} + \boldsymbol{\zeta}^{(\ell)} \mathbf{E}^{(\ell)}, \quad (12)$$

where  $\boldsymbol{\varepsilon}$  is the strain vector;  $\boldsymbol{\sigma}^{(\ell)}$  is the stress vector;  $\mathbf{E}^{(\ell)}$  is the electric field vector;  $\mathbf{D}^{(\ell)}$  is the electric displacement vector;  $\mathbf{A}^{(\ell)}$  is the elastic compliance matrix;  $\mathbf{d}^{(\ell)}$  is the piezoelectric matrix;  $\boldsymbol{\zeta}^{(\ell)}$  is the dielectric matrix defined by

$$\begin{aligned} \boldsymbol{\varepsilon} &= [\varepsilon_{11} \ \varepsilon_{22} \ \varepsilon_{33} \ 2\varepsilon_{23} \ 2\varepsilon_{13} \ 2\varepsilon_{12}]^T, \\ \boldsymbol{\sigma}^{(\ell)} &= [\sigma_{11}^{(\ell)} \ \sigma_{22}^{(\ell)} \ \sigma_{33}^{(\ell)} \ \sigma_{23}^{(\ell)} \ \sigma_{13}^{(\ell)} \ \sigma_{12}^{(\ell)}]^T, \\ \mathbf{E}^{(\ell)} &= [E_1^{(\ell)} \ E_2^{(\ell)} \ E_3^{(\ell)}]^T, \quad \mathbf{D}^{(\ell)} = [D_1^{(\ell)} \ D_2^{(\ell)} \ D_3^{(\ell)}]^T, \\ \mathbf{A}^{(\ell)} &= \begin{bmatrix} A_{11}^{(\ell)} & A_{12}^{(\ell)} & A_{13}^{(\ell)} & 0 & 0 & A_{16}^{(\ell)} \\ & A_{22}^{(\ell)} & A_{23}^{(\ell)} & 0 & 0 & A_{26}^{(\ell)} \\ & & A_{33}^{(\ell)} & 0 & 0 & A_{36}^{(\ell)} \\ & & & A_{44}^{(\ell)} & A_{45}^{(\ell)} & 0 \\ & & & & A_{55}^{(\ell)} & 0 \\ \text{sym.} & & & & & A_{66}^{(\ell)} \end{bmatrix}, \\ \mathbf{d}^{(\ell)} &= \begin{bmatrix} 0 & 0 & 0 & d_{14}^{(\ell)} & d_{15}^{(\ell)} & 0 \\ 0 & 0 & 0 & d_{24}^{(\ell)} & d_{25}^{(\ell)} & 0 \\ d_{31}^{(\ell)} & d_{32}^{(\ell)} & d_{33}^{(\ell)} & 0 & 0 & d_{36}^{(\ell)} \end{bmatrix}, \\ \boldsymbol{\zeta}^{(\ell)} &= \begin{bmatrix} \zeta_{11}^{(\ell)} & \zeta_{12}^{(\ell)} & 0 \\ & \zeta_{22}^{(\ell)} & 0 \\ \text{sym.} & & \zeta_{33}^{(\ell)} \end{bmatrix}. \end{aligned} \quad (13)$$

As we remember, the index of the piezoelectric layer  $\ell = i_1, i_2, \dots, i_L$ . Solving constitutive equations (11) for stresses and substituting stresses in constitutive equations (12), one obtains

$$\boldsymbol{\sigma}^{(\ell)} = \mathbf{C}^{(\ell)} \boldsymbol{\varepsilon} - (\mathbf{e}^{(\ell)})^T \mathbf{E}^{(\ell)}, \quad (14)$$

$$\mathbf{D}^{(\ell)} = \mathbf{e}^{(\ell)} \boldsymbol{\varepsilon} + \boldsymbol{\epsilon}^{(\ell)} \mathbf{E}^{(\ell)}, \quad (15)$$

where  $\mathbf{C}^{(\ell)}$  is the material stiffness matrix;  $\mathbf{e}^{(\ell)}$  and  $\boldsymbol{\epsilon}^{(\ell)}$  are the piezoelectric and dielectric matrices expressed as

$$\begin{aligned} \mathbf{C}^{(\ell)} &= (\mathbf{A}^{(\ell)})^{-1}, \quad \mathbf{e}^{(\ell)} = \mathbf{d}^{(\ell)} \mathbf{C}^{(\ell)}, \\ \boldsymbol{\varepsilon}^{(\ell)} &= \boldsymbol{\zeta}^{(\ell)} - \mathbf{d}^{(\ell)} \mathbf{C}^{(\ell)} (\mathbf{d}^{(\ell)})^T. \end{aligned} \quad (16)$$

## 5 Hu-Washizu variational equation for 9-parameter piezoelectric shell formulation

A higher-order 9-parameter piezoelectric ESL shell theory developed is based on the approximations of displacements (1), displacement-dependent strains (4), electric potential (7) and electric field (10) in the thickness direction. Additionally, to circumvent shear and membrane locking, we introduce the similar approximation for the assumed displacement-independent strains  $\hat{\boldsymbol{\varepsilon}}_{ij}$ , that is,

$$\hat{\boldsymbol{\varepsilon}}_{ij} = \sum_I L^I \hat{\boldsymbol{\varepsilon}}_{ij}^I, \quad (17)$$

where  $\hat{\boldsymbol{\varepsilon}}_{ij}^I(\boldsymbol{\theta}_1, \boldsymbol{\theta}_2)$  are the displacement-independent strains of I-surfaces.

Substituting approximations (1), (4), (7), (10) and (17) into the 3D Hu-Washizu functional [Kulikova and Plotnikova (2008b)] and introducing stress-resultants

$$H_{ij}^I = \sum_n \int_{z_{n-1}}^{z_n} \boldsymbol{\sigma}_{ij}^{(n)} L^I d\boldsymbol{\theta}_3, \quad (18)$$

and invoking the stationarity of this functional with respect to independent variables, one derives the following mixed variational equation for the 9-parameter piezoelectric EG solid-shell element formulation:

$$\begin{aligned} & \int_{-1}^1 \int_{-1}^1 \left\{ \sum_I \left[ \delta(\hat{\boldsymbol{\varepsilon}}^I)^T \left( \mathbf{H}^I - \sum_J \mathbf{D}_{uu}^{IJ} \hat{\boldsymbol{\varepsilon}}^J + \mathbf{D}_{u\varphi}^{(\ell)I} \tilde{\mathbf{E}}^{(\ell)} \right) \right. \right. \\ & \left. \left. + \delta(\mathbf{H}^I)^T (\hat{\boldsymbol{\varepsilon}}^I - \boldsymbol{\varepsilon}^I) - \delta(\boldsymbol{\varepsilon}^I)^T \mathbf{H}^I \right] \right. \\ & \left. + \delta(\tilde{\mathbf{E}}^{(\ell)})^T \left[ \sum_I \left( \mathbf{D}_{u\varphi}^{(\ell)I} \right)^T \hat{\boldsymbol{\varepsilon}}^I + \mathbf{D}_{\varphi\varphi}^{(\ell)} \tilde{\mathbf{E}}^{(\ell)} \right] \right. \\ & \left. + \delta \mathbf{v}^T \mathbf{p} + \delta \boldsymbol{\chi}_\ell^T \mathbf{q}_\ell \right\} A_1 A_2 c_1^M c_2^M \ell_1 \ell_2 d\xi_1 d\xi_2 + \delta W_{el} = 0. \end{aligned} \quad (19)$$

Here, convenient matrix notations are introduced

$$\mathbf{v} = [u_1^- \ u_2^- \ u_3^- \ u_1^M \ u_2^M \ u_3^M \ u_1^+ \ u_2^+ \ u_3^+]^T,$$

$$\boldsymbol{\varepsilon}^I = [\boldsymbol{\varepsilon}_{11}^I \ \boldsymbol{\varepsilon}_{22}^I \ \boldsymbol{\varepsilon}_{33}^I \ 2\boldsymbol{\varepsilon}_{12}^I \ 2\boldsymbol{\varepsilon}_{13}^I \ 2\boldsymbol{\varepsilon}_{23}^I]^T,$$

$$\hat{\boldsymbol{\varepsilon}}^I = [\hat{\boldsymbol{\varepsilon}}_{11}^I \ \hat{\boldsymbol{\varepsilon}}_{22}^I \ \hat{\boldsymbol{\varepsilon}}_{33}^I \ 2\hat{\boldsymbol{\varepsilon}}_{12}^I \ 2\hat{\boldsymbol{\varepsilon}}_{13}^I \ 2\hat{\boldsymbol{\varepsilon}}_{23}^I]^T,$$

$$\mathbf{H}^I = [H_{11}^I \ H_{22}^I \ H_{33}^I \ H_{12}^I \ H_{13}^I \ H_{23}^I]^T,$$

$$\tilde{\boldsymbol{\epsilon}}^{(\ell)} = [E_1^{(\ell)-} \ E_1^{(\ell)+} \ E_2^{(\ell)-} \ E_2^{(\ell)+} \ E_3^{(\ell)}]^T,$$

$$\mathbf{p} = [-p_1^- \ -p_2^- \ -p_3^- \ 0 \ 0 \ 0 \ p_1^+ \ p_2^+ \ p_3^+]^T,$$

$$\boldsymbol{\chi}_\ell = [\varphi_\ell^- \ \varphi_\ell^+]^T, \quad \mathbf{q}_\ell = [q_\ell^- \ q_\ell^+]^T, \quad (20)$$

where  $\mathbf{D}_{uu}^{IJ}$ ,  $\mathbf{D}_{u\varphi}^{(\ell)I}$  and  $\mathbf{D}_{\varphi\varphi}^{(\ell)}$  are the mechanical, piezoelectric and dielectric constitutive matrices presented in Appendix A;  $\xi_\alpha = (\theta_\alpha - d_\alpha) / \ell_\alpha$  are the normalized curvilinear elemental coordinates depicted in Figure 2;  $d_\alpha$  are the coordinates of the center of the element;  $2\ell_\alpha$  are the lengths of the element in  $\theta_\alpha$ -directions;  $c_\alpha^M$  are the components of the shifter tensor at the midsurface, see Eq. 6;  $p_i^-$  and  $p_i^+$  are the tractions applied to the bottom and top surfaces of the shell;  $q_\ell^-$  and  $q_\ell^+$  are the prescribed surface charge densities of the  $\ell$ th piezoelectric layer;  $W_{el}$  is the work done by external loads acting on the edge boundary surface  $\Sigma_{el}$ .

**Remark 1.** For the simplicity, we limit our discussion to the case of one piezoelectric layer, i.e.,  $L = 1$  and  $\ell = i_1 \in \{1, 2, \dots, N\}$  since only a sign of the summation needs to be involved in Eq. 19 to generalize. Besides, it is assumed that metrics of all I-surfaces are identical and equal to the metric of the midsurface.

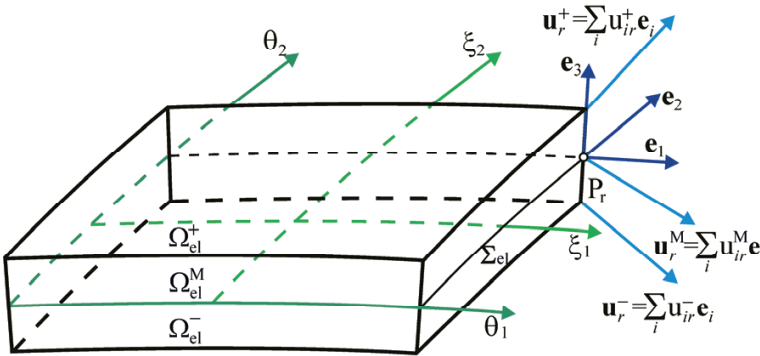


Figure 2: Piezoelectric EG solid-shell element based on the 9-parameter ESL shell model in the case of choosing the midsurface as a reference surface, where  $P_r$  is the element node ( $r = 1, 2, \dots, NN$ )

## 6 Modified assumed natural strain method

The finite element formulation is based on the simple and efficient approximation of shells via piezoelectric EG four-node solid-shell elements

$$\mathbf{v} = \sum_r N_r \mathbf{v}_r, \quad (21)$$

$$\mathbf{v}_r = [u_{1r}^- \ u_{2r}^- \ u_{3r}^- \ u_{1r}^M \ u_{2r}^M \ u_{3r}^M \ u_{1r}^+ \ u_{2r}^+ \ u_{3r}^+]^T,$$

$$N_r = \frac{1}{4} (1 + n_{1r} \xi_1) (1 + n_{2r} \xi_2),$$

$$n_{1r} = \begin{cases} 1 & \text{for } r = 1, 4 \\ -1 & \text{for } r = 2, 3 \end{cases}, \quad n_{2r} = \begin{cases} 1 & \text{for } r = 1, 2 \\ -1 & \text{for } r = 3, 4 \end{cases},$$

$$\boldsymbol{\chi}^\ell = \sum_r N_r \boldsymbol{\chi}_{\ell r}, \quad \boldsymbol{\chi}_{\ell r} = [\varphi_{\ell r}^- \ \varphi_{\ell r}^+]^T, \quad (22)$$

where  $N_r(\xi_1, \xi_2)$  are the bilinear shape functions of the element;  $\mathbf{v}_r$  and  $\boldsymbol{\chi}_{\ell r}$  are the displacement and electric potential vectors of the element nodes; the index  $r$  runs from 1 to 4 and denotes the number of nodes.

To implement the analytical integration throughout the element, we employ the assumed interpolations of natural strains and electric field vectors [Kulikov and Plotnikova (2006, 2007, 2011)]

$$\boldsymbol{\varepsilon}^I = \sum_r N_r \boldsymbol{\varepsilon}_r^I, \quad \boldsymbol{\varepsilon}_r^I = \boldsymbol{\varepsilon}^I(\mathbf{P}_r), \quad (23)$$

$$\tilde{\mathbf{E}}^{(\ell)} = \sum_r N_r \tilde{\mathbf{E}}_r^{(\ell)}, \quad \tilde{\mathbf{E}}_r^{(\ell)} = \tilde{\mathbf{E}}^{(\ell)}(\mathbf{P}_r), \quad (24)$$

where  $\boldsymbol{\varepsilon}_r^I$  are the strain vectors of I-surfaces at element nodes;  $\tilde{\mathbf{E}}_r^{(\ell)}$  are the electric field vectors at element nodes.

**Remark 2.** The main idea of such approach can be traced back to the ANS method [see, e.g. Bathe and Dvorkin (1986), Park and Stanley (1986)]. In contrast with above formulations, we treat the term ‘‘ANS method’’ in a broader sense. In our piezoelectric EG solid-shell element formulation, all components of the Green-Lagrange strain tensor are assumed to vary bilinearly inside the element. This implies that instead of expected non-linear interpolation the more suitable bilinear ANS interpolation is utilized. It should be noticed that we advocate the use of the modified ANS method (23) for all components of the Green-Lagrange strain tensor to implement the efficient analytical integration throughout the element.

Introducing further the displacement and electric potential vectors of the shell element

$$\mathbf{U} = [\mathbf{v}_1^T \mathbf{v}_2^T \mathbf{v}_3^T \mathbf{v}_4^T]^T, \quad (25)$$

$$\Phi_\ell = [\chi_{\ell 1}^T \chi_{\ell 2}^T \chi_{\ell 3}^T \chi_{\ell 4}^T]^T, \quad (26)$$

one derives the following expressions for nodal strain and electric field vectors:

$$\boldsymbol{\varepsilon}_r^I = \mathbf{B}_r^I \mathbf{U} + \mathbf{A}_r^I(\mathbf{U}) \mathbf{U}, \quad (27)$$

$$\tilde{\mathbf{E}}_r^{(\ell)} = -\mathbf{B}_r^{(\ell)} \Phi_\ell, \quad (28)$$

where  $\mathbf{B}_r^I$  and  $\mathbf{A}_r^I(\mathbf{U})$  are the *constant* inside the element nodal matrices of order  $6 \times 36$  corresponding to the linear and non-linear strain-displacement transformations;  $\mathbf{B}_r^{(\ell)}$  are the *constant* inside the element nodal matrices of order  $5 \times 8$  corresponding to the electric field transformation (10). The explicit presentations of nodal matrices  $\mathbf{B}_r^I$ ,  $\mathbf{A}_r^I(\mathbf{U})$  and  $\mathbf{B}_r^{(\ell)}$  can be found following a technique developed by Kulikov and Plotnikova (2011), in particular,

$$\mathbf{B}_r^I = \begin{bmatrix} c_{1r}^I (\boldsymbol{\Lambda}_{11r}^I)^T \\ c_{2r}^I (\boldsymbol{\Lambda}_{22r}^I)^T \\ (\boldsymbol{\Lambda}_{33r}^I)^T \\ c_{1r}^I (\boldsymbol{\Lambda}_{12r}^I)^T + c_{2r}^I (\boldsymbol{\Lambda}_{21r}^I)^T \\ c_{1r}^I (\boldsymbol{\Lambda}_{13r}^I)^T + (\boldsymbol{\Lambda}_{31r}^I)^T \\ c_{2r}^I (\boldsymbol{\Lambda}_{23r}^I)^T + (\boldsymbol{\Lambda}_{32r}^I)^T \end{bmatrix}, \quad \mathbf{A}_r^I(\mathbf{U}) = \begin{bmatrix} \mathbf{U}^T \boldsymbol{\Pi}_{11r}^I \\ \mathbf{U}^T \boldsymbol{\Pi}_{22r}^I \\ \mathbf{U}^T \boldsymbol{\Pi}_{33r}^I \\ \mathbf{U}^T \boldsymbol{\Pi}_{12r}^I \\ \mathbf{U}^T \boldsymbol{\Pi}_{13r}^I \\ \mathbf{U}^T \boldsymbol{\Pi}_{23r}^I \end{bmatrix},$$

$$\boldsymbol{\Pi}_{ijr}^I = \frac{1}{2} \sum_m \boldsymbol{\Lambda}_{mir}^I (\boldsymbol{\Lambda}_{mjr}^I)^T \text{ for } i = j,$$

$$\boldsymbol{\Pi}_{ijr}^I = \frac{1}{2} \sum_m \left[ \boldsymbol{\Lambda}_{mir}^I (\boldsymbol{\Lambda}_{mjr}^I)^T + \boldsymbol{\Lambda}_{mjr}^I (\boldsymbol{\Lambda}_{mir}^I)^T \right] \text{ for } i < j, \quad (29)$$

where  $c_{\alpha r}^I = 1 + k_{\alpha r} z^I$  are the nodal values of the shifter tensor at I-surfaces;  $\boldsymbol{\Lambda}_{ijr}^I$  are the *constant* inside the element column matrices of order  $36 \times 1$  given in Appendix B.

From the computational point of view it is convenient to rewrite the ANS interpolations (23) and (24) as follows:

$$\boldsymbol{\varepsilon}^I = \sum_{r_1, r_2} (\xi_1)^{r_1} (\xi_2)^{r_2} \boldsymbol{\varepsilon}^{I r_1 r_2}, \quad \boldsymbol{\varepsilon}^{I r_1 r_2} = \mathbf{B}^{I r_1 r_2} \mathbf{U} + \mathbf{A}^{I r_1 r_2}(\mathbf{U}) \mathbf{U}, \quad (30)$$

$$\tilde{\mathbf{E}}^{(\ell)} = \sum_{r_1, r_2} (\xi_1)^{r_1} (\xi_2)^{r_2} \boldsymbol{\epsilon}^{(\ell)r_1 r_2}, \quad \boldsymbol{\epsilon}^{(\ell)r_1 r_2} = -\mathbf{B}^{(\ell)r_1 r_2} \boldsymbol{\Phi}_\ell. \quad (31)$$

Here and in the following developments the indices  $r_1, r_2$  take the values 0 and 1, and the additional notations are introduced

$$\mathbf{B}^{I00} = \frac{1}{4} (\mathbf{B}'_1 + \mathbf{B}'_2 + \mathbf{B}'_3 + \mathbf{B}'_4),$$

$$\mathbf{B}^{I01} = \frac{1}{4} (\mathbf{B}'_1 + \mathbf{B}'_2 - \mathbf{B}'_3 - \mathbf{B}'_4),$$

$$\mathbf{B}^{I10} = \frac{1}{4} (\mathbf{B}'_1 - \mathbf{B}'_2 - \mathbf{B}'_3 + \mathbf{B}'_4),$$

$$\mathbf{B}^{I11} = \frac{1}{4} (\mathbf{B}'_1 - \mathbf{B}'_2 + \mathbf{B}'_3 - \mathbf{B}'_4).$$

Matrices  $\mathbf{B}^{(\ell)r_1 r_2}$  and  $\mathbf{A}^{I r_1 r_2}(\mathbf{U})$  are written in a similar way by using nodal matrices  $\mathbf{B}_r^{(\ell)}$  and  $\mathbf{A}_r^I(\mathbf{U})$ .

### 7 Hybrid stress-strain method

To improve the computational efficiency of low-order EG solid-shell elements, a hybrid method can be applied. It is well established now that “the hybrid method in structural mechanics is defined at the one which is formulated by multivariable variational functional, yet the resulting matrix equations consist of only the nodal values of displacements as unknown” [Pian (1995)].

Thus, to avoid shear and membrane locking and have no spurious zero energy modes, the assumed displacement-independent strains and stress resultants fields throughout the element are invoked

$$\hat{\boldsymbol{\epsilon}}^I = \sum_{r_1+r_2 < 2} (\xi_1)^{r_1} (\xi_2)^{r_2} \mathbf{Q}^{r_1 r_2} \hat{\boldsymbol{\epsilon}}^{I r_1 r_2},$$

$$\hat{\boldsymbol{\epsilon}}^{I00} = [\hat{\boldsymbol{\epsilon}}_{11}^{I00} \hat{\boldsymbol{\epsilon}}_{22}^{I00} \hat{\boldsymbol{\epsilon}}_{33}^{I00} 2\hat{\boldsymbol{\epsilon}}_{12}^{I00} 2\hat{\boldsymbol{\epsilon}}_{13}^{I00} 2\hat{\boldsymbol{\epsilon}}_{23}^{I00}]^T,$$

$$\hat{\boldsymbol{\epsilon}}^{I01} = [\hat{\boldsymbol{\epsilon}}_{11}^{I01} \hat{\boldsymbol{\epsilon}}_{33}^{I01} 2\hat{\boldsymbol{\epsilon}}_{13}^{I01}]^T, \quad \hat{\boldsymbol{\epsilon}}^{I10} = [\hat{\boldsymbol{\epsilon}}_{22}^{I10} \hat{\boldsymbol{\epsilon}}_{33}^{I10} 2\hat{\boldsymbol{\epsilon}}_{23}^{I10}]^T \quad (32)$$

and

$$\mathbf{H}^I = \sum_{r_1+r_2 < 2} (\xi_1)^{r_1} (\xi_2)^{r_2} \mathbf{Q}^{r_1 r_2} \mathbf{H}^{I r_1 r_2},$$

$$\mathbf{H}^{I00} = [H_{11}^{I00} H_{22}^{I00} H_{33}^{I00} H_{12}^{I00} H_{13}^{I00} H_{23}^{I00}]^T,$$

$$\begin{aligned} \mathbf{H}^{I01} &= [H_{11}^{I01} H_{33}^{I01} H_{13}^{I01}]^T, \\ \mathbf{H}^{I10} &= [H_{22}^{I10} H_{33}^{I10} H_{23}^{I10}]^T, \end{aligned} \tag{33}$$

where  $\mathbf{Q}^{r_1 r_2}$  are the projective matrices defined as

$$\begin{aligned} \mathbf{Q}^{00} &= \begin{bmatrix} 1 & 0 & 0 & 0 & 0 & 0 \\ 0 & 1 & 0 & 0 & 0 & 0 \\ 0 & 0 & 1 & 0 & 0 & 0 \\ 0 & 0 & 0 & 1 & 0 & 0 \\ 0 & 0 & 0 & 0 & 1 & 0 \\ 0 & 0 & 0 & 0 & 0 & 1 \end{bmatrix}, \\ \mathbf{Q}^{01} &= \begin{bmatrix} 1 & 0 & 0 \\ 0 & 0 & 0 \\ 0 & 1 & 0 \\ 0 & 0 & 0 \\ 0 & 0 & 1 \\ 0 & 0 & 0 \end{bmatrix}, \quad \mathbf{Q}^{10} = \begin{bmatrix} 0 & 0 & 0 \\ 1 & 0 & 0 \\ 0 & 1 & 0 \\ 0 & 0 & 0 \\ 0 & 0 & 0 \\ 0 & 0 & 1 \end{bmatrix}. \end{aligned} \tag{34}$$

This approach was developed for the purely mechanical geometrically non-linear 6- and 7- parameter EG solid-shell element formulations by Kulikov and Plotnikova (2006, 2007, 2008a, 2009).

Substituting interpolations (21), (22), (30)-(33) into the Hu-Washizu variational equation (19) and integrating *analytically* throughout the element, one obtains the elemental equilibrium equations of the developed piezoelectric finite element formulation

$$\hat{\boldsymbol{\epsilon}}^{Ir_1 r_2} = (\mathbf{Q}^{r_1 r_2})^T [B^{Ir_1 r_2} + \mathbf{A}^{Ir_1 r_2}(\mathbf{U})] \mathbf{U} \text{ for } r_1 + r_2 < 2, \tag{35}$$

$$\begin{aligned} \mathbf{H}^{Ir_1 r_2} &= \sum_J (\mathbf{Q}^{r_1 r_2})^T \mathbf{D}_{uu}^{IJ} \mathbf{Q}^{r_1 r_2} \hat{\boldsymbol{\epsilon}}^{Jr_1 r_2} \\ &+ (\mathbf{Q}^{r_1 r_2})^T \mathbf{D}_{u\varphi}^{(\ell)I} \mathbf{B}^{(\ell)r_1 r_2} \boldsymbol{\Phi}_\ell \text{ for } r_1 + r_2 < 2, \end{aligned} \tag{36}$$

$$\sum_{r_1+r_2 < 2} \frac{1}{3^{r_1+r_2}} \sum_I [B^{Ir_1 r_2} + 2\mathbf{A}^{Ir_1 r_2}(\mathbf{U})]^T \mathbf{Q}^{r_1 r_2} \mathbf{H}^{Ir_1 r_2} = \mathbf{F}_p, \tag{37}$$

$$\begin{aligned} &\sum_{r_1+r_2 < 2} \frac{1}{3^{r_1+r_2}} \sum_I \left( \mathbf{B}^{(\ell)r_1 r_2} \right)^T \left( \mathbf{D}_{u\varphi}^{(\ell)I} \right)^T \mathbf{Q}^{r_1 r_2} \hat{\boldsymbol{\epsilon}}^{Ir_1 r_2} \\ &- \sum_{r_1, r_2} \frac{1}{3^{r_1+r_2}} \left( \mathbf{B}^{(\ell)r_1 r_2} \right)^T \mathbf{D}_{\varphi\varphi}^{(\ell)} \mathbf{B}^{(\ell)r_1 r_2} \boldsymbol{\Phi}_\ell = \mathbf{F}_q^{(\ell)}, \end{aligned} \tag{38}$$

where  $\mathbf{F}_p$  is the element-wise surface traction vector;  $\mathbf{F}_q^{(\ell)}$  is the element-wise electric force vector of the  $\ell$ th piezoelectric layer.

**Remark 3.** In order to carry out the analytical integration, we have supposed that a product  $A_1 A_2 c_1^M c_2^M$  in Eq. 19 is constant throughout the element and is evaluated at the element center.

For the actuator-embedded shell analysis when only a prescribed input voltage is applied, the non-linear finite element equations are simplified because Eq. 38 can be omitted. Employing further the Newton-Raphson iteration process

$$\begin{aligned} \mathbf{U}^{[k+1]} &= \mathbf{U}^{[k]} + \Delta \mathbf{U}^{[k]}, \quad \hat{\boldsymbol{\epsilon}}^{I r_1 r_2 [k+1]} = \hat{\boldsymbol{\epsilon}}^{I r_1 r_2 [k]} + \Delta \hat{\boldsymbol{\epsilon}}^{I r_1 r_2 [k]}, \\ \mathbf{H}^{I r_1 r_2 [k+1]} &= \mathbf{H}^{I r_1 r_2 [k]} + \Delta \mathbf{H}^{I r_1 r_2 [k]} \quad (k = 0, 1, \dots) \end{aligned} \quad (39)$$

and eliminating displacement-independent strains  $\Delta \hat{\boldsymbol{\epsilon}}^{I r_1 r_2 [k]}$  and stress resultants  $\Delta \mathbf{H}^{I r_1 r_2 [k]}$  from linearized equilibrium equations derived, we arrive at the governing finite element equations

$$\mathbf{K}_T \Delta \mathbf{U}^{[k]} = \Delta \mathbf{F}^{[k]}, \quad (40)$$

where  $\mathbf{K}_T = \mathbf{K}_D + \mathbf{K}_H$  is the tangent stiffness matrix;  $\Delta \mathbf{F}^{[k]}$  is the right hand side vector given by

$$\mathbf{K}_D = \sum_{r_1+r_2 < 2} \frac{1}{3^{r_1+r_2}} \sum_{I,J} \left( \mathbf{L}^{I r_1 r_2 [k]} \right)^T \mathbf{D}_{uu}^{I J r_1 r_2} \mathbf{L}^{J r_1 r_2 [k]}, \quad (41)$$

$$\mathbf{K}_H = 2 \sum_{r_1+r_2 < 2} \frac{1}{3^{r_1+r_2}} \sum_I \mathbf{R}^{I r_1 r_2} \left( \mathbf{Q}^{r_1 r_2} \mathbf{H}^{I r_1 r_2 [k]} \right), \quad (42)$$

$$\begin{aligned} \Delta \mathbf{F}^{[k]} &= \mathbf{F}_p - \sum_{r_1+r_2 < 2} \frac{1}{3^{r_1+r_2}} \left\{ \sum_{I,J} \left( \mathbf{L}^{I r_1 r_2 [k]} \right)^T \mathbf{D}_{uu}^{I J r_1 r_2} \left[ \mathbf{L}^{J r_1 r_2 [k]} \right. \right. \\ &\quad \left. \left. - \mathbf{A}^{J r_1 r_2} \left( \mathbf{U}^{[k]} \right) \right] U^{[k]} + \sum_I \left( \mathbf{L}^{I r_1 r_2 [k]} \right)^T \mathbf{Q}^{r_1 r_2} \boldsymbol{\Xi}_\ell^{I r_1 r_2} \right\}, \end{aligned} \quad (43)$$

where

$$\mathbf{L}^{I r_1 r_2 [k]} = \mathbf{B}^{I r_1 r_2} + 2 \mathbf{A}^{I r_1 r_2} \left( \mathbf{U}^{[k]} \right),$$

$$\boldsymbol{\Xi}_\ell^{I r_1 r_2} = \left( \mathbf{Q}^{r_1 r_2} \right)^T \mathbf{D}_{u\varphi}^{(\ell) I} \mathbf{B}^{(\ell) r_1 r_2} \boldsymbol{\Phi}_\ell,$$

$$\bar{\mathbf{D}}_{uu}^{I J r_1 r_2} = \left( \mathbf{Q}^{r_1 r_2} \right)^T \mathbf{D}_{uu}^{I J} \mathbf{Q}^{r_1 r_2}, \quad \mathbf{D}_{uu}^{I J r_1 r_2} = \mathbf{Q}^{r_1 r_2} \bar{\mathbf{D}}_{uu}^{I J r_1 r_2} \left( \mathbf{Q}^{r_1 r_2} \right)^T,$$

$$\mathbf{R}^{I r_1 r_2}(\mathbf{H}^I) = \sum_{i \leq j} \mathbf{H}_{ij}^I \boldsymbol{\Pi}_{ij}^{I r_1 r_2} \text{ for } r_1 + r_2 < 2,$$

$$\boldsymbol{\Pi}_{ij}^{I 00} = \frac{1}{4} (\boldsymbol{\Pi}_{ij1}^I + \boldsymbol{\Pi}_{ij2}^I + \boldsymbol{\Pi}_{ij3}^I + \boldsymbol{\Pi}_{ij4}^I),$$

$$\boldsymbol{\Pi}_{ij}^{I 01} = \frac{1}{4} (\boldsymbol{\Pi}_{ij1}^I + \boldsymbol{\Pi}_{ij2}^I - \boldsymbol{\Pi}_{ij3}^I - \boldsymbol{\Pi}_{ij4}^I),$$

$$\boldsymbol{\Pi}_{ij}^{I 10} = \frac{1}{4} (\boldsymbol{\Pi}_{ij1}^I - \boldsymbol{\Pi}_{ij2}^I - \boldsymbol{\Pi}_{ij3}^I + \boldsymbol{\Pi}_{ij4}^I). \quad (44)$$

To find the tangent stiffness matrix, a useful matrix transformation

$$[\mathbf{A}^{I r_1 r_2}(\mathbf{U})]^T \mathbf{H}^I = \mathbf{R}^{I r_1 r_2}(\mathbf{H}^I) \mathbf{U} \text{ for } r_1 + r_2 < 2 \quad (45)$$

should be invoked.

**Remark 4.** As expected, the tangent stiffness matrix is symmetric. This is due to the fact that both matrices  $\mathbf{K}_D$  and  $\mathbf{K}_H$  are symmetric. The proof of symmetry of the latter matrix follows from Eqs. 29 and 44.

For computing the mode stress resultant vectors from Eq. 42 at the  $k$ th iteration step, we employ the advanced finite element technique, that is

$$\mathbf{H}^{I r_1 r_2 [k]} = \sum_J \bar{\mathbf{D}}^{J r_1 r_2} \hat{\boldsymbol{\epsilon}}^{J r_1 r_2 [k]} + \boldsymbol{\Xi}_\ell^{I r_1 r_2} \text{ for } r_1 + r_2 < 2, \quad (46)$$

$$\hat{\boldsymbol{\epsilon}}^{I r_1 r_2 [k]} = (\mathbf{Q}^{r_1 r_2})^T [\mathbf{B}^{I r_1 r_2} \mathbf{U}^{[k]} + 2\mathbf{A}^{I r_1 r_2} (\mathbf{U}^{[k-1]}) \Delta \mathbf{U}^{[k-1]} + \mathbf{A}^{I r_1 r_2} (\mathbf{U}^{[k-1]}) \mathbf{U}^{[k-1]}] \text{ for } r_1 + r_2 < 2, \quad (47)$$

where  $\Delta \mathbf{U}^{[k-1]} = \mathbf{U}^{[k]} - \mathbf{U}^{[k-1]}$ . Note that Eq. 47 holds for  $k \geq 1$ , whereas at the beginning of the iteration process one should set

$$\Delta \mathbf{U}^{[0]} = \mathbf{0} \text{ and } \hat{\boldsymbol{\epsilon}}^{I r_1 r_2 [0]} = \mathbf{0}. \quad (48)$$

The proposed approach allows the use of load steps, which are much larger than possible with standard EG displacement-based solid-shell element formulations. This is because of the fact that an additional load vector due to compatibility mismatch (47) at the  $k$ th iteration is present in linearized equilibrium equations (40) and disappears only at the end of the iteration process.

The equilibrium equations (40) for each element are assembled by the usual technique to form the global equilibrium equations. These equations have to be performed until the required accuracy of the solution can be obtained. A displacement-based convergence criterion employed herein can be described as

$$\left\| U_G^{[k+1]} - U_G^{[k]} \right\| < \varepsilon \left\| U_G^{[k]} \right\|, \quad (49)$$

where  $\|\bullet\|$  stands for the Euclidean norm;  $U_G$  is the global displacement vector;  $\epsilon$  is the prescribed tolerance.

### 8 Benchmark problems

The performance of the proposed non-linear piezoelectric EG four-node solid-shell element EG9P4 is evaluated with several discriminating problems extracted from the literature and authors' example as well. For this purpose the following notations are introduced: NStep is the number of load steps; NIter is the total number of Newton iterations.

#### 8.1 Slit ring plate under line load

This example was presented by Basar and Ding (1990) to test the non-linear finite element formulations for thin-walled shell structures and further has been extensively used by many investigators. The ring plate is subjected to a line load  $P$  applied at its free edge of the slit, while the other edge is fully clamped (Figure 3).

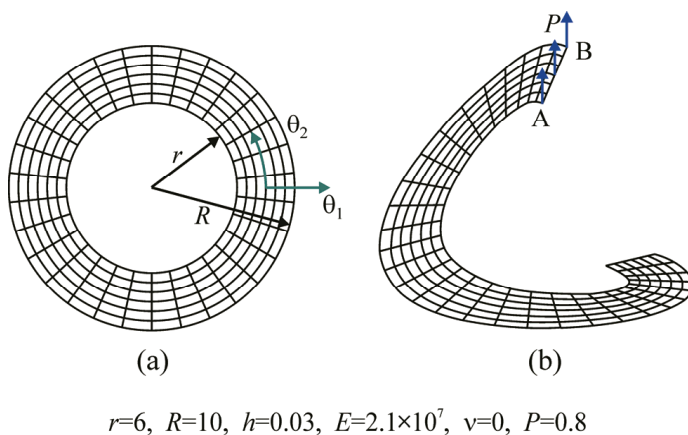


Figure 3: Slit ring plate under the line load: (a) geometry and (b) deformed configuration (modeled by  $6 \times 30$  mesh)

The displacements at points A and B of the plate, presented in Table 1 and Figure 4, have been found by employing uniform meshes of EG9P4 elements. A comparison with the purely mechanical 6-parameter EG four-node solid-shell element EG6P4 [Kulikov and Plotnikova (2006)] and isoparametric four-node solid-shell element [Sze, Chan and Pian (2002)] is also given. As can be seen, coarse mesh configurations with the EG9P4 element can be used because the  $2 \times 5$  mesh already yields

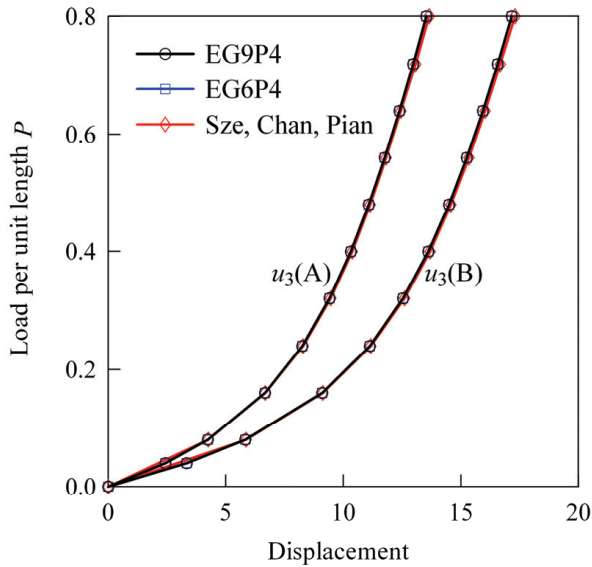


Figure 4: Midplane displacements of the slit ring plate (modeled by  $6 \times 30$  mesh)

96 % of the reference solution provided by Sze, Chan and Pian (2002). Note also that in this case only 8 Newton iterations are needed to find a converged solution with the chosen criterion and tolerance.

## 8.2 Cantilever laminated plate with segmented actuators

Consider a cantilever laminated plate with segmented PZT G1195 actuators attached to its bottom and top surfaces [Crawley and Lazarus (1991)] as shown in Figure 5. The plate core is composed of six AS4/3501 graphite/epoxy layers with a stacking sequence  $[0/45/-45]_s$ . The geometrical data of the problem are taken to be  $a = 292$  mm,  $b = 152$  mm,  $h_C = 0.83$  mm and  $h_{PZT} = 0.25$  mm. The non-vanishing material parameters for graphite/epoxy are  $E_1 = 143$  GPa,  $E_2 = E_3 = 9.7$  GPa,  $G_{12} = G_{13} = 6$  GPa,  $G_{23} = 2$  GPa,  $\nu_{12} = \nu_{13} = \nu_{23} = 0.3$  and for PZT G1195 are  $E = 63$  GPa,  $G = 24.2$  GPa,  $\nu = 0.3$ ,  $d_{31} = d_{32} = 0.254$  nm/V,  $d_{15} = d_{24} = 0.584$  nm/V,  $d_{33} = 0.374$  nm/V.

The piezoceramic layers are polarized in opposite directions parallel to the thickness direction and subjected to opposite electric potentials  $-\hat{\phi}$  and  $\hat{\phi}$  to the outer patches surfaces to induce the bending actuation. The electrodes on the interfaces are grounded. A plate is modeled by the non-uniform  $16 \times 10$  mesh of EG9P4 elements depicted in Figure 5.

8.2.1 Geometrically linear plate response

Figure 6 displays the distribution of dimensionless midplane displacements  $w_1 = u_3^M(B)/b$  and  $w_2 = (u_3^M(C) - u_3^M(A))/b$  along the  $x$ -axis. A comparison with the isoparametric piezoelectric four-node solid-shell element formulation [Tan and Vu-Quoc (2005)] and experimental study [Crawley and Lazarus (1991)] is also given. The results are presented for a plate loaded statically by a constant voltage of 157.6 V. It is seen that both four-node solid-shell elements perform excellently.

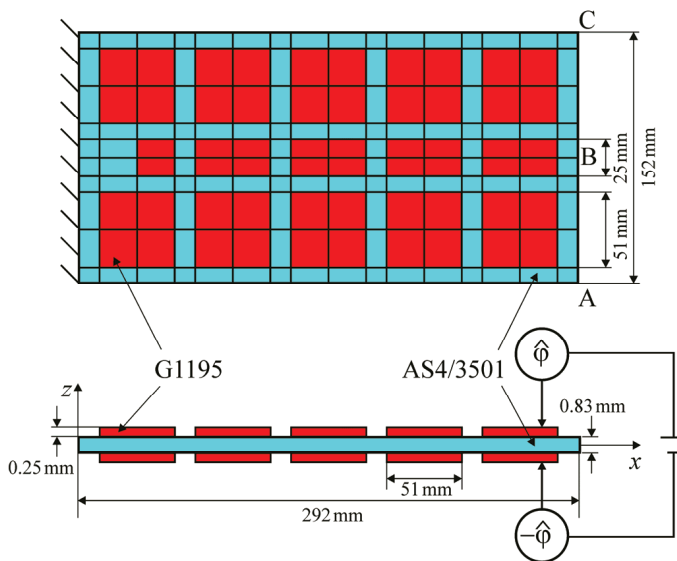


Figure 5: Cantilever plate with segmented actuators: geometry and mesh configuration

8.2.2 Geometrically non-linear plate response

For the finite deformation analysis, we apply the electric potential  $\hat{\phi} = 1576$  V. Figure 7 shows a voltage-displacement curve compared with a finite element solution [Tan and Vu-Quoc (2005)]. One can observe that again all results agree closely but the EG9P4 element is less expensive owing to the economical derivation of its stiffness matrix. Moreover, the EG9P4 element requires only one load step to find a converged solution of the problem.



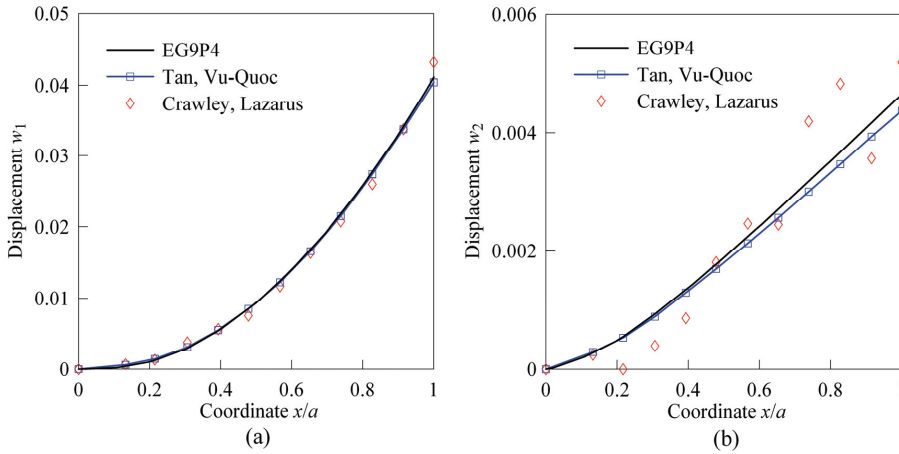


Figure 6: Dimensionless displacements of the cantilever plate subjected to a constant voltage  $\hat{\phi} = 157.6 \text{ V}$ : (a)  $w_1$  and (b)  $w_2$

### 8.3 Spiral actuator

Consider a spiral actuator made of the PZT-5H ceramic with the following properties:  $c_{11} = c_{22} = 127.205 \text{ GPa}$ ,  $c_{12} = 80.212 \text{ GPa}$ ,  $c_{13} = c_{23} = 84.670 \text{ GPa}$ ,  $c_{33} = 117.436 \text{ GPa}$ ,  $c_{44} = c_{55} = 22.988 \text{ GPa}$ ,  $c_{66} = 23.474 \text{ GPa}$ ,  $e_{31} = e_{32} = -6.62 \text{ C/m}^2$ ,  $e_{33} = 23.24 \text{ C/m}^2$ ,  $e_{24} = e_{15} = 17.03 \text{ C/m}^2$ . The spiral, shown in Figure 8, consists of four turns and has external radii  $r_{\min} = 1.875 \text{ mm}$  and  $r_{\max} = 15.2 \text{ mm}$ , an effective length  $L = 215 \text{ mm}$ , a thickness  $h = 0.2 \text{ mm}$  and a width  $b = 3.75 \text{ mm}$ . The geometrical parameters of the spiral shell can be represented as

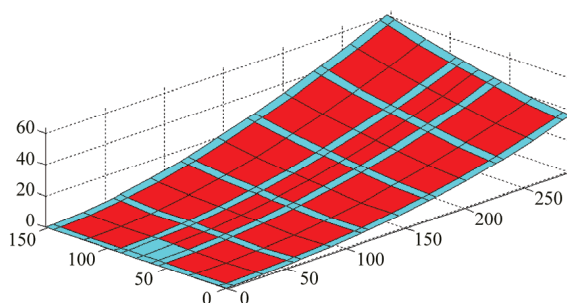
$$A_1 = 1, \quad A_2 = \sqrt{a^2 + r^2}, \quad k_1 = 0, \quad k_2 = \frac{1}{A_2^3} (2a^2 + r^2),$$

$$r = r_{\min} + a\theta_2, \quad \theta_2 \in [0, 8\pi], \quad (50)$$

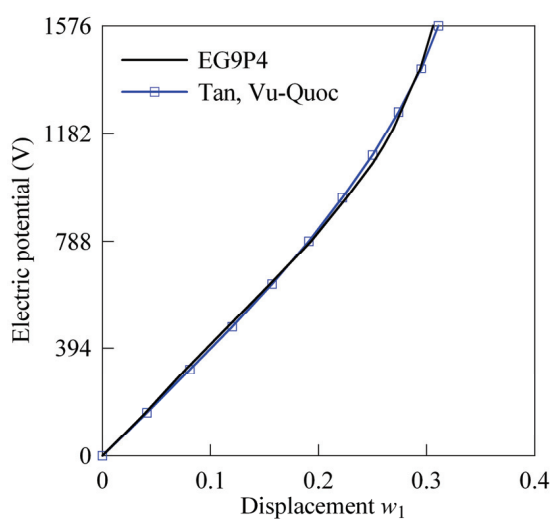
where  $r$  is the polar radius;  $a$  is the parameter, which controls the distance between successive turnings.

#### 8.3.1 Geometrically linear actuator response

A spiral actuator is polarized in the thickness direction and subjected to a constant voltage  $\Delta\phi = 100 \text{ V}$ . The shell is modeled by uniform meshes of EG9P4 elements. Table 3 lists the results of the convergence study due to mesh refinement considering the tangential and transverse midsurface displacements at the tip and a comparison with two finite element solutions [Zouari, Ben Zineb and Benjeddou (2009)].



(a)



(b)

Figure 7: Cantilever plate: (a) deformed configuration at applied voltage  $\hat{\phi} = 1576$  V and (b) non-linear voltage-displacement curve

The reference solution is provided by the Abaqus solid element C3D8E with a fine mesh, that is, two elements across the thickness and 20 elements across the width but the number of elements across the length is not documented. As can be seen, the EG9P4 element allows us to utilize coarse meshes because the  $1 \times 16$  mesh yields already a good answer for the tangential displacement. It should be noted that the 9-parameter shell model overestimates the tangential tip displacement by 40 %. This can be explained by the fact that the layer-wise description with fictitious interfaces inside the shell body has to be employed. A comparison with the degenerated-shell element Q<sub>4</sub>TSF [Zouari, Ben Zineb and Benjeddou (2009)]

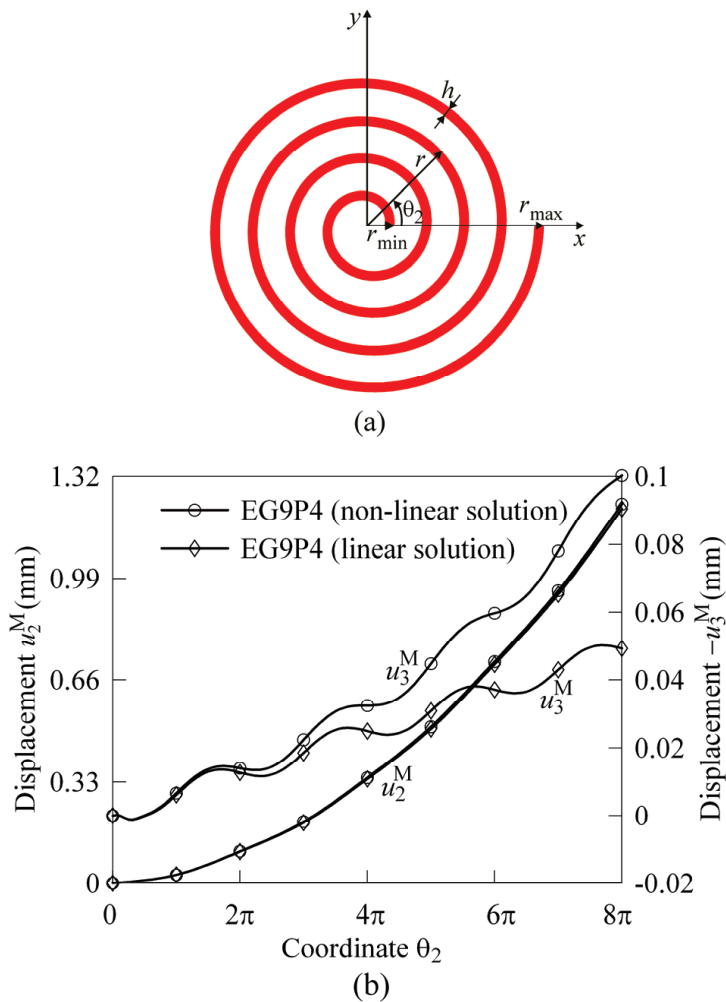


Figure 8: Spiral actuator: (a) geometry and (b) dependence of midsurface displacements on the circumferential coordinate under electric potential  $\Delta\varphi = 2000\text{V}$

shows additionally that the  $d_{33}$ -effect is of great importance for the analysis of deep actuators.

### 8.3.2 Geometrically non-linear actuator response

For the non-linear shell analysis, the actuator is loaded statically by the extremely high electric potential  $\Delta\varphi = 2000\text{V}$  and modeled by the uniform mesh  $1 \times 128$  of

Table 2: Midsurface displacements at the tip of the spiral actuator subjected to a constant voltage  $\Delta\phi = 100V$

Element	EG9P4										Q4TSF	C3D8E
	1×16	2×16	4×16	1×32	2×32	4×32	1×64	1×128				
Mesh												
$-u_3^M$ ( $\mu m$ )	2.0959	2.1004	2.1013	2.6190	2.6236	2.6239	2.5043	2.4645	2.00	2.59		
$u_2^M$ ( $\mu m$ )	58.160	58.169	58.166	59.926	59.894	59.886	60.546	60.725	-0.62	41.47		

Table 3: Midsurface displacements at points A and C of the pinched three-layer hyperbolic shell with piezoelectric patches under purely mechanical loading using uniform meshes of EG9P4 elements and criterion (49) with tolerance of  $10^{-4}$

Mesh	$4 \times 4$	$8 \times 8$	$16 \times 16$	$32 \times 32$	$64 \times 64$
$-u_y(\text{A})$	1.9237	2.3317	2.4190	2.4451	2.4526
$u_y(\text{C})$	1.7993	1.9551	1.9615	1.9628	1.9631
NStep/NIter	1/6	1/5	1/6	1/6	1/6

EG solid-shell elements developed. Figure 8 displays the distribution of tangential and transverse midsurface displacements in the  $\theta_2$ -direction. It is of interest to notice that a geometrically linear 9-parameter shell model provides very reliable results for the most important tangential displacement at the tip. Note that again the EG9P4 element requires only one load step to find a converged solution.

#### 8.4 Laminated hyperbolic shell with piezoelectric patches

Consider a three-layer cross-ply hyperbolic shell under two pairs of opposite forces. This problem was studied by Basar, Ding and Schultz (1993) for testing the finite rotation shell formulations, while we employ a hyperbolic shell example to assess the possibility of controlling the shape of laminated shells with segmented piezoelectric patches subjected to arbitrarily large actuation. Such an example is also an excellent test to verify the proper representation of inextensional bending and the ability of the element to model large rigid-body motions.

The shell core is composed of three composite layers with ply thicknesses of  $[h_1/h_2/h_3]$ , where  $h_n = h_C/3$ , and ply orientations of  $[90/0/90]$ , that is, fiber directions coincide with the  $\theta_2$ -direction in outer layers. The shape control of the three-layer hyperbolic shell is achieved with the help of eight piezoelectric patches of the thickness  $h_{PZT} = 0.01$  cm attached at inner and outer surfaces and located at the force point as depicted in Figure 9. The geometrical data of the shell and the material properties of the composite are taken to be typical in the finite element literature:  $r = 7.5$  cm,  $R = 15$  cm,  $L = 20$  cm,  $h_C = 0.04$  cm and  $E_1 = 4 \times 10^7$  N / cm<sup>2</sup>,  $E_2 = E_3 = 10^6$  N / cm<sup>2</sup>,  $G_{12} = G_{13} = G_{23} = 6 \times 10^5$  N / cm<sup>2</sup>,  $\nu_{12} = \nu_{13} = \nu_{23} = 0.25$ . The non-vanishing material parameters of piezoceramic layers are  $E = 20$  GPa,  $G = 7.7$  GPa,  $\nu = 0.3$ ,  $d_{31} = d_{32} = 2$  nm / V. The piezoceramic patches are polarized in opposite directions parallel to the thickness direction and subjected to a constant voltage  $\hat{\phi}$  to induce the bending actuation. As usual the electrodes on interfaces are grounded.

Due to symmetry of the problem, only one octant of the shell is discretized with the  $16 \times 16$  mesh of EG9P4 elements. Figure 10 displays undeformed and deformed

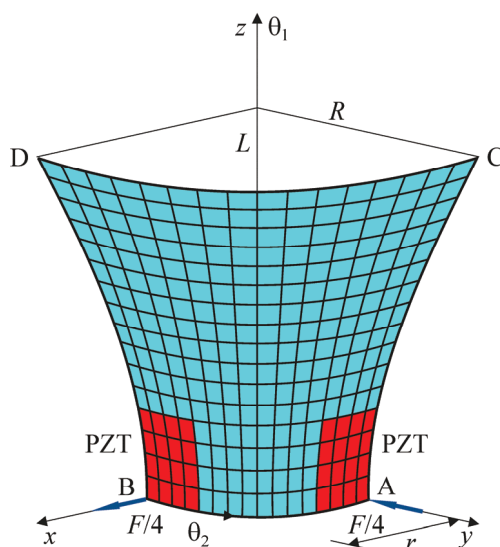


Figure 9: One octant of the three-layer hyperbolic shell with segmented actuators: geometry and mesh configuration

configurations of the shell under mechanical loading  $F = 200\text{ N}$  and electrical loading  $\hat{\phi} = 1000\text{ V}$  and  $1960\text{ V}$  as well. It is seen that the electric potential of  $1960\text{ V}$  applied to outer patches surfaces returns a shell to its initial configuration. To investigate a problem of the shape control more carefully, we represent in Figure 11 the midsurface displacements at points A, B, C and D, where  $u_x$  and  $u_y$  denote displacements in  $x$ - and  $y$ -directions. Additionally, Table 3 lists the results of the convergence study due to mesh refinement.

## 9 Conclusions

A new finite rotation piezoelectric laminated solid-shell model has been developed. This model is based on the objective strain-displacement relationships of the 9-parameter ESL shell theory, which are invariant under arbitrarily large rigid-body shell motions. The simple and efficient hybrid stress-strain piezoelectric EG four-node solid-shell element is based on the original approach in which displacement vectors of outer and middle surfaces are introduced but resolved, in contrast with the isoparametric solid-shell element formulation, in the reference surface frame. This model is robust because permits one, first, to employ much larger load steps than existing piezoelectric shell element models and, second, to utilize the com-

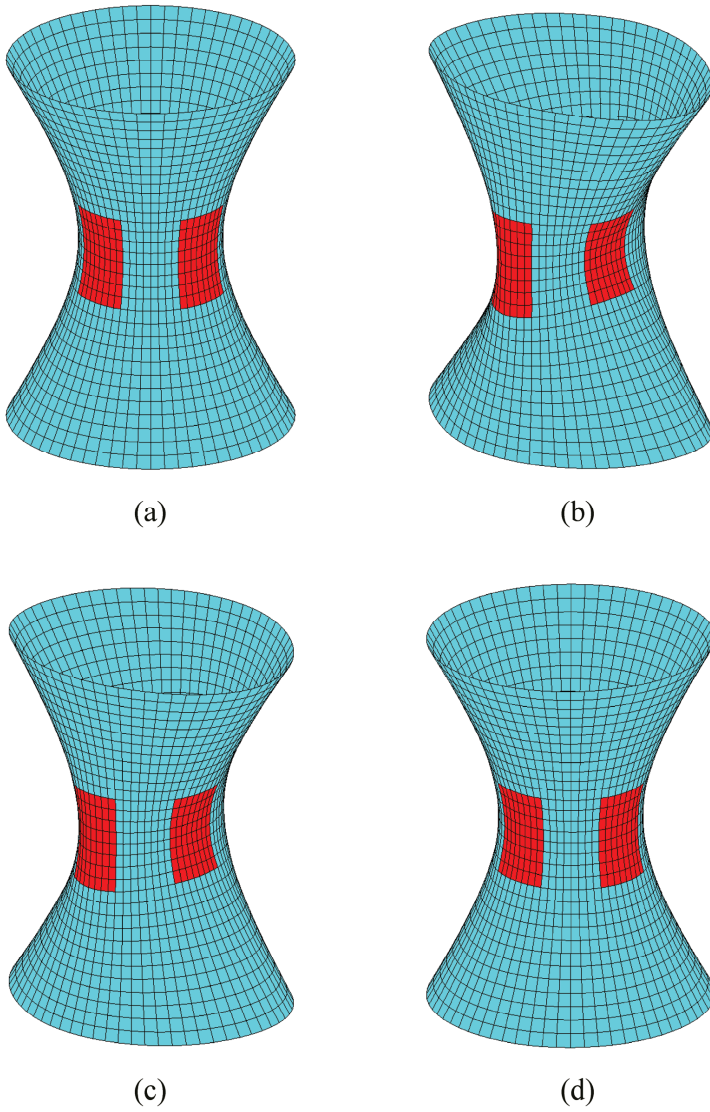


Figure 10: Three-layer hyperbolic shell at applied loads: (a)  $F = 0$  and  $\hat{\phi} = 0$ , (b)  $F = 200\text{ N}$  and  $\hat{\phi} = 0$ , (c)  $F = 200\text{ N}$  and  $\hat{\phi} = 1000\text{ V}$ , and (d)  $F = 200\text{ N}$  and  $\hat{\phi} = 1960\text{ V}$

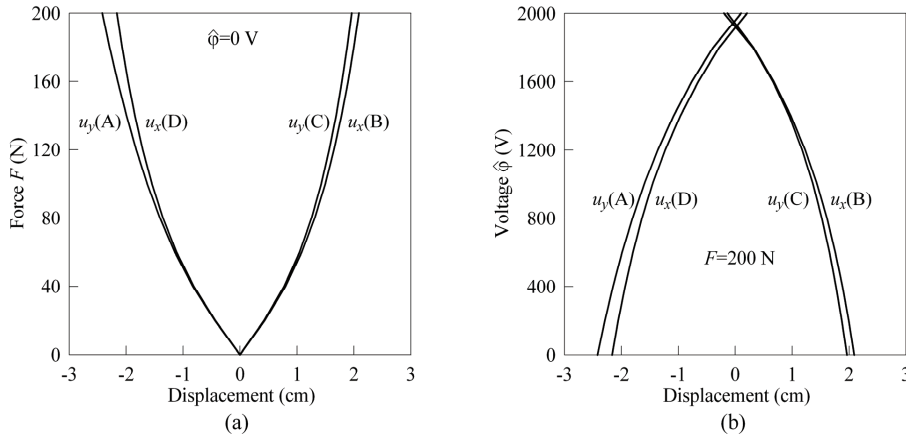


Figure 11: Three-layer hyperbolic shell. Midsurface displacements at points A, B, C and D versus: (a) force  $F$  for  $\hat{\phi} = 0$  and (b) voltage  $\hat{\phi}$  for  $F = 200$  N

plete 3D constitutive equations. It is remarkable that the tangent stiffness matrix requires only direct substitutions and is evaluated by employing the 3D analytical integration. It is necessary to note also that the EG9P4 element allows the use of very coarse meshes even in shell problems with extremely large displacements and rotations.

**Acknowledgement:** The support of this work by Russian Ministry of Education and Science under Grant No 2.1.1/660 and No 2.1.1/10003 is gratefully acknowledged.

**Appendix A**

The mechanical, piezoelectric and dielectric constitutive matrices introduced in section 5 are given by

$$\mathbf{D}_{uu}^{IJ} = \begin{bmatrix} D_{11}^{IJ} & D_{12}^{IJ} & D_{13}^{IJ} & D_{16}^{IJ} & 0 & 0 \\ & D_{22}^{IJ} & D_{23}^{IJ} & D_{26}^{IJ} & 0 & 0 \\ & & D_{33}^{IJ} & D_{36}^{IJ} & 0 & 0 \\ & & & D_{66}^{IJ} & 0 & 0 \\ & & & & D_{55}^{IJ} & D_{54}^{IJ} \\ \text{sym.} & & & & & D_{44}^{IJ} \end{bmatrix},$$

$$\mathbf{D}_{u\varphi}^{(\ell)I} = \begin{bmatrix} 0 & 0 & 0 & 0 & \eta_\ell^I e_{31}^{(\ell)} \\ 0 & 0 & 0 & 0 & \eta_\ell^I e_{32}^{(\ell)} \\ 0 & 0 & 0 & 0 & \eta_\ell^I e_{33}^{(\ell)} \\ 0 & 0 & 0 & 0 & \eta_\ell^I e_{36}^{(\ell)} \\ \eta_\ell^{0I} e_{15}^{(\ell)} & \eta_\ell^{1I} e_{15}^{(\ell)} & \eta_\ell^{0I} e_{25}^{(\ell)} & \eta_\ell^{1I} e_{25}^{(\ell)} & 0 \\ \eta_\ell^{0I} e_{14}^{(\ell)} & \eta_\ell^{1I} e_{14}^{(\ell)} & \eta_\ell^{0I} e_{24}^{(\ell)} & \eta_\ell^{1I} e_{24}^{(\ell)} & 0 \end{bmatrix},$$

$$\mathbf{D}_{\varphi\varphi}^{(\ell)} = \begin{bmatrix} \kappa_\ell^{00} \in_{11}^{(\ell)} & \kappa_\ell^{01} \in_{11}^{(\ell)} & \kappa_\ell^{00} \in_{12}^{(\ell)} & \kappa_\ell^{01} \in_{12}^{(\ell)} & 0 \\ & \kappa_\ell^{11} \in_{11}^{(\ell)} & \kappa_\ell^{01} \in_{12}^{(\ell)} & \kappa_\ell^{11} \in_{12}^{(\ell)} & 0 \\ & & \kappa_\ell^{00} \in_{22}^{(\ell)} & \kappa_\ell^{01} \in_{22}^{(\ell)} & 0 \\ & & & \kappa_\ell^{11} \in_{22}^{(\ell)} & 0 \\ \text{sym.} & & & & h_\ell \in_{33}^{(\ell)} \end{bmatrix}.$$

Here,

$$D_{ab}^{IJ} = \sum_n \mu_n^{IJ} C_{ab}^{(n)}, \quad \mu_n^{IJ} = \int_{z_{n-1}}^{z_n} L^I L^J d\theta_3,$$

$$\eta_\ell^I = \int_{z_{\ell-1}}^{z_\ell} L^I d\theta_3, \quad \eta_\ell^{pI} = \int_{z_{\ell-1}}^{z_\ell} (N_\ell^-)^{1-p} (N_\ell^+)^p L^I d\theta_3,$$

$$\kappa_\ell^{pq} = \int_{z_{\ell-1}}^{z_\ell} (N_\ell^-)^{2-p-q} (N_\ell^+)^{p+q} d\theta_3,$$

where the indices used take the following values:  $a, b = 1, 2, \dots, 6$  and  $p, q = 0, 1$ .

## Appendix B

The column matrices  $\mathbf{\Lambda}_{ijr}^I$  of order  $36 \times 1$  introduced in section 6 are evaluated as follows:

$$\left(\mathbf{\Lambda}_{\alpha\alpha r}^I\right)_{\alpha+3K+9(s-1),1} = d_{\alpha r s},$$

$$\left(\mathbf{\Lambda}_{\alpha\alpha r}^I\right)_{\beta+3K+9(s-1),1} = \delta_{rs} B_{\beta s} \text{ for } \beta \neq \alpha,$$

$$\left(\mathbf{\Lambda}_{\alpha\alpha r}^I\right)_{3+3K+9(s-1),1} = \delta_{rs} k_{\alpha s},$$

$$\left(\mathbf{\Lambda}_{\beta\alpha r}^I\right)_{\beta+3K+9(s-1),1} = d_{\alpha r s},$$

$$\left(\mathbf{\Lambda}_{\beta\alpha r}^I\right)_{\alpha+3K+9(s-1),1} = -\delta_{rs}B_{\beta s} \text{ for } \beta \neq \alpha,$$

$$\left(\mathbf{\Lambda}_{3\alpha r}^I\right)_{3+3K+9(s-1),1} = d_{\alpha rs},$$

$$\left(\mathbf{\Lambda}_{3\alpha r}^I\right)_{\alpha+3K+9(s-1),1} = -\delta_{rs}k_{\alpha s},$$

$$\left(\mathbf{\Lambda}_{i3r}^I\right)_{i+9(s-1),1} = \delta_{rs}(2K-3)/h,$$

$$\left(\mathbf{\Lambda}_{i3r}^I\right)_{3+i+9(s-1),1} = 4\delta_{rs}(1-K)/h,$$

$$\left(\mathbf{\Lambda}_{i3r}^I\right)_{6+i+9(s-1),1} = \delta_{rs}(2K-1)/h,$$

$$d_{\alpha rs} = \frac{1}{4\ell_{\alpha}A_{\alpha r}}n_{\alpha s}(1+n_{\beta r}n_{\beta s}) \text{ for } \beta \neq \alpha,$$

where  $A_{\alpha r}$ ,  $k_{\alpha r}$  and  $B_{\alpha r}$  are the nodal values of the geometrical parameters of the reference surface;  $\delta_{rs}$  is the Kronecker delta;  $K = 0, 1$  and  $2$  for  $I = -, M$  and  $+$ , respectively; parameters  $n_{\alpha s}$  are defined by Eq. 21 and, as we remember, the indices  $r, s$  run from 1 to 4. The remaining components of column matrices not written out explicitly are zero.

## References

- Arciniega, R. A.; Reddy, J. N.** (2007): Tensor-based finite element formulation for geometrically nonlinear analysis of shell structures. *Computer Methods in Applied Mechanics and Engineering*, vol. 196, pp. 1048-1073.
- Bathe, K. J.; Dvorkin, E. N.** (1986): A formulation of general shell elements - the use of mixed interpolation of tensorial components. *International Journal for Numerical Methods in Engineering*, vol. 22, pp. 697-722.
- Basar, Y.; Ding, Y.** (1990): Finite-rotation elements for the non-linear analysis of thin shell structures. *International Journal of Solids and Structures*, vol. 26, pp. 83-97.
- Basar, Y.; Ding, Y.; Schultz, R.** (1993): Refined shear-deformation models for composite laminates with finite rotations. *International Journal of Solids and Structures*, vol. 30, pp. 2611-2638.
- Benjeddou, A.; Deü, J.-F.; Letombe, S.** (2002): Free vibrations of simply-supported piezoelectric adaptive plates: an exact sandwich formulation. *Thin-Walled Structures*, vol. 40, pp. 573-593.
- Brank, B.** (2005): Nonlinear shell models with seven kinematic parameters. *Computer Methods in Applied Mechanics and Engineering*, vol. 194, pp. 2336-2362.

**Brank, B.; Ibragimbegovic, A.; Bohinc, U.** (2008): On prediction of 3d stress state in elastic shell by higher-order shell formulations. *CMES: Computer Modeling in Engineering & Sciences*, vol. 33, pp. 85-108.

**Buchter, N.; Ramm, E.; Roehl, D.** (1994): Three-dimensional extension of non-linear shell formulation based on the enhanced assumed strain concept. *International Journal for Numerical Methods in Engineering*, vol. 37, pp. 2551-2568.

**Crawley, E. F.; Lazarus, K. B.** (1991): Induced strain actuation of isotropic and anisotropic plates. *AIAA Journal*, vol. 29, pp. 944-951.

**El-Abbasi, N.; Meguid, S. A.** (2000): A new shell element accounting for through-thickness deformation. *Computer Methods in Applied Mechanics and Engineering*, vol. 189, pp. 841-862.

**Gopinathan, S. V.; Varadan, V. V.; Varadan, V. K.** (2000): A review and critique of theories for piezoelectric laminates. *Smart Materials and Structures*, vol. 9, pp. 24-48.

**Klinkel, S.; Wagner, W.** (2006): A geometrically non-linear piezoelectric solid shell element based on a mixed multi-field variational formulation. *International Journal for Numerical Methods in Engineering*, vol. 65, pp. 349-382.

**Klinkel, S.; Wagner, W.** (2008): A piezoelectric solid shell element based on a mixed variational formulation for geometrically linear and nonlinear applications. *Computers & Structures*, vol. 86, pp. 38-46.

**Kulikov, G. M.** (2001): Refined global approximation theory of multilayered plates and shells. *Journal of Engineering Mechanics*, vol. 127, pp. 119-125.

**Kulikov, G. M.; Carrera, E.** (2008): Finite deformation higher-order shell models and rigid-body motions. *International Journal of Solids and Structures*, vol. 45, pp. 3153-3172.

**Kulikov, G. M.; Plotnikova, S. V.** (2002): Investigation of locally loaded multilayered shells by mixed finite-element method. 2. Geometrically nonlinear statement. *Mechanics of Composite Materials*, vol. 38, pp. 539-546.

**Kulikov, G. M.; Plotnikova, S. V.** (2004): Finite deformation plate theory and large rigid-body motions. *International Journal of Non-Linear Mechanics*, vol. 39, pp. 1093-1109.

**Kulikov, G. M.; Plotnikova, S. V.** (2006): Non-linear strain-displacement equations exactly representing large rigid-body motions. Part II. Enhanced finite element technique. *Computer Methods in Applied Mechanics and Engineering*, vol. 195, pp. 2209-2230.

**Kulikov, G. M.; Plotnikova, S. V.** (2007): Non-linear geometrically exact assumed stress-strain four-node solid-shell element with high coarse-mesh accuracy. *Finite*

*Elements in Analysis and Design*, vol. 43, pp. 425-443.

**Kulikov, G. M.; Plotnikova, S. V.** (2008a): Finite rotation geometrically exact four-node solid-shell element with seven displacement degrees of freedom. *CMES: Computer Modeling in Engineering & Sciences*, vol. 28, pp. 15-38.

**Kulikov, G. M.; Plotnikova, S. V.** (2008b): Geometrically exact four-node piezoelectric solid-shell element. *Mechanics of Advanced Materials and Structures*, vol. 15, pp. 199-207.

**Kulikov, G. M.; Plotnikova, S. V.** (2009): Calculation of composite structures subjected to follower loads by using a geometrically exact shell element. *Mechanics of Composite Materials*, vol. 45, pp. 545-556.

**Kulikov, G. M.; Plotnikova, S. V.** (2011): Exact geometry piezoelectric solid-shell element based on the 7-parameter model. *Mechanics of Advanced Materials and Structures*, vol. 18, in print.

**Lee, K.; Lee S. W.** (2008): An assumed strain solid shell element formulation with transversely quadratic displacement, *CMES: Computer Modeling in Engineering & Sciences*, vol. 34, pp. 253-272.

**Lentzen, S.** (2009): *Nonlinearly Coupled Thermopiezoelectric Modelling and FE-Simulation of Smart Structures*. Fortschritt-Berichte VDI, Reihe 20, Nr. 419. Düsseldorf: VDI Verlag.

**Parisch, H.** (1995): A continuum-based shell theory for non-linear applications. *International Journal for Numerical Methods in Engineering*, vol. 38, pp.1855-1883.

**Park, K. C.; Stanley, G. M.** (1986): A curved  $C^0$  shell element based on assumed natural coordinate strains. *Journal of Applied Mechanics*, vol. 53, pp. 278-290.

**Pian, T. H. H.** (1995): State-of-the-art development of hybrid/mixed finite element method. *Finite Elements in Analysis and Design*, vol. 21, pp. 5-20.

**Sansour, C.** (1995): A theory and finite element formulation of shells at finite deformations involving thickness change: circumventing the use of a rotation tensor. *Archive of Applied Mechanics*, vol. 65, pp. 194-216.

**Sze, K. Y.; Chan, W. K.; Pian, T. H. H.** (2002): An eight-node hybrid-stress solid-shell element for geometric non-linear analysis of elastic shells. *International Journal for Numerical Methods in Engineering*, vol. 55, pp. 853-878.

**Sze, K. Y.; Yang, X.-M.; Fan, H.** (2004): Electric assumption for piezoelectric laminate analysis. *International Journal of Solids and Structures*, vol. 41, pp. 2363-2382.

**Tan, X. G.; Vu-Quoc, L.** (2005): Optimal solid shell element for large deformable composite structures with piezoelectric layers and active vibration control. *Inter-*

*national Journal for Numerical Methods in Engineering*, vol. 64, pp. 1981-2013.

**Zouari, W.; Ben Zineb, T.; Benjeddou, A.** (2009): A FSDT-MITC piezoelectric shell finite element with ferroelectric non-linearity. *Journal of Intelligent Material Systems and Structures*, vol. 20, pp. 2055-2075.